



OPEN

# Optimization of process parameters for trimethoprim and sulfamethoxazole removal by magnetite-chitosan nanoparticles using Box–Behnken design

Mahsa Alishiri<sup>1</sup>, Maryam Gonbadi<sup>2</sup>, Mehdi Narimani<sup>2</sup>, Seyyed Amirreza Abdollahi<sup>3✉</sup> & Negin Shahsavaripour<sup>4</sup>

The contamination of the aquatic environment with antibiotics is among the major and developing problems worldwide. The present study investigates the potential of adsorbent magnetite-chitosan nanoparticles ( $\text{Fe}_3\text{O}_4/\text{CS}$  NPs) for removing trimethoprim (TMP) and sulfamethoxazole (SMX). For this purpose,  $\text{Fe}_3\text{O}_4/\text{CS}$  NPs were synthesized by the co-precipitation method, and the adsorbent characteristics were investigated using XRD, SEM, TEM,  $\text{pH}_{\text{zpc}}$ , FTIR, and VSM. The effect of independent variables (pH, sonication time, adsorbent amount, and analyte concentration) on removal performance was modeled and evaluated by Box–Behnken design (BBD). The SEM image of the  $\text{Fe}_3\text{O}_4/\text{CS}$  adsorbent showed that the adsorbent had a rough and irregular surface. The size of  $\text{Fe}_3\text{O}_4/\text{CS}$  crystals was about 70 nm. XRD analysis confirmed the purity and absence of impurities in the adsorbent. TEM image analysis showed that the adsorbent had a porous structure, and the particle size was in the range of nanometers. In VSM, the saturation magnetization of  $\text{Fe}_3\text{O}_4/\text{CS}$  adsorbent was  $25 \text{ emu g}^{-1}$  and the magnet could easily separate the adsorbent from the solution. The results revealed that the optimum condition was achieved at a concentration of  $22 \text{ mg L}^{-1}$ , a sonication time of 15 min, an adsorbent amount of  $0.13 \text{ g}/100 \text{ mL}$ , and a pH of 6. Among different solvents (i.e., ethanol, acetone, nitric acid, and acetonitrile), significant desorption of TMP and SMX was achieved using ethanol. Also, results confirmed that  $\text{Fe}_3\text{O}_4/\text{CS}$  NPs can be used for up to six adsorption/desorption cycles. In addition, applying the  $\text{Fe}_3\text{O}_4/\text{CS}$  NPs on real water samples revealed that  $\text{Fe}_3\text{O}_4/\text{CS}$  NPs could remove TMP and SMX in the 91.23–95.95% range with RSD ( $n = 3$ )  $< 4$ . Overall, the  $\text{Fe}_3\text{O}_4/\text{CS}$  NPs exhibit great potential for removing TMP and SMX antibiotics from real water samples.

Antibiotics are a large group of pharmaceutical substances that kill bacteria or slow their growth. They have extensive applications in medical infection treatment, accounting for approximately 15% of total drug consumption<sup>1–3</sup>. An important point to consider is that less than 10% of these drugs undergo any transformation in the body, while the rest are excreted unchanged<sup>4–6</sup>. Antibiotics can find their way into the environment through various pathways, including discharge from manufacturing sites, domestic and hospital wastewater, gradual disposal of expired medications, topical application of drugs, and washing off drugs from the skin or contaminated clothes<sup>7–9</sup>.

The combination of trimethoprim (TMP) and sulfamethoxazole (SMX) as cotrimoxazole is present in several pharmaceutical forms, including oral suspension, tablets, and intravenous infusion for human or veterinary use. This combination is widely used to treat urinary tract and respiratory infections<sup>10–12</sup>. Environmental issues due to releasing TMP and SMX antibiotics into water sources pose a serious threat. Their most significant impact lies

<sup>1</sup>Department of Biomedical Engineering, University of Illinois Chicago, Chicago, USA. <sup>2</sup>Nanochemical Engineering Department, Faculty of Advanced Technologies, Shiraz University, Shiraz, Iran. <sup>3</sup>Faculty of Mechanical Engineering, University of Tabriz, Tabriz, Iran. <sup>4</sup>Technical and Engineering Faculty, Islamic Azad University, Sirjan, Iran. ✉email: abdollahisseyedamirreza@gmail.com; s.amirreza.abdollahi1401@ms.tabrizu.ac.ir

in the toxicity to micro-organisms present in the environment, disrupting ecological balance<sup>13</sup>. TMP and SMX antibiotics can also be used as liquid manure or sewage sludge fertilizers, entering aquatic environments, soil, and the food chain, leading to microbial resistance against them<sup>14</sup>. Consequently, drug resistance may occur in individuals, making common antibiotics ineffective in responding to infections in the body<sup>15</sup>.

Several methods have been employed for the removal of antibiotic from water. These techniques include reverse osmosis, ion exchange, coagulation, membrane filtration, and adsorption<sup>16–19</sup>. However, specific approaches have not been considered due to their associated limitations, including the need for extensive maintenance, high energy, chemical consumption, and suboptimal efficiency. Adsorption is one of the most widely used techniques in wastewater treatment processes due to its simplicity and relatively low cost<sup>20</sup>. During adsorption, dissolved ions or compounds are adsorbed and remain on the adsorbent solid surface<sup>21</sup>.

Recently, nanomaterials have garnered significant attention as exceptional adsorbents, primarily due to their high specific surface area and numerous active groups. Additionally, certain nanoparticles can selectively adsorb specific compounds, making them highly versatile for diverse chemical groups<sup>22,23</sup>. Over the past two decades, research on the exceptional electrical, catalytic, optical, and magnetic properties of nanoparticles has progressed rapidly<sup>24</sup>. Among the different types of nanoparticles, metal nanoparticles have attracted considerable attention due to their unique physical and chemical properties, including their ability to penetrate into microscopic pores, colloidal stability, and resistance to aggregation in solutions<sup>25,26</sup>.

As a subset of metal nanoparticles, magnetic nanoparticles can be easily separated from solutions using an magnet, eliminating the need for centrifugation and filtration. Hematite ( $\alpha$ -Fe<sub>2</sub>O<sub>3</sub>), magnetite (Fe<sub>3</sub>O<sub>4</sub>), and maghemite ( $\gamma$ -Fe<sub>2</sub>O<sub>3</sub>) are important members of the Iron family because of their anti-corrosion properties, adjustable optical and magnetic characteristics, excellent chemical stability, cost-effectiveness, and environmental friendliness<sup>27,28</sup>. Among the adsorbents, magnetite-chitosan nanoparticles (Fe<sub>3</sub>O<sub>4</sub>/CS NPs) have been used to remove pollutants from aqueous environments because of the high potential, high adsorption capacity, and high specific surface area of these nanoparticles<sup>29,30</sup>.

In a study, Karimi et al. used Fe<sub>3</sub>O<sub>4</sub>/CS nano-bio-adsorbent to remove Cd (II), Cu (II), and Zn (II) ions from an aqueous solution. The removal rate for Cd (II), Cu (II), and Zn (II) ions was 99.98%, 93.69%, and 83.81%, respectively, at pH of 5.3, a metal concentration of 10 mg L<sup>-1</sup>, the adsorbent dosage of 1 g L<sup>-1</sup>, and room temperature for 24 h<sup>31</sup>. Thinh et al. used Fe<sub>3</sub>O<sub>4</sub>/CS NPs to remove Cr (VI) from the aqueous solution. The results revealed that the highest adsorption capacity of 55.80 mg g<sup>-1</sup> was obtained at a pH of 3 for 100 min at room temperature<sup>32</sup>. In another study, Shen et al. evaluated the removal of C. I. Acid Red 73 by magnetic chitosan-Fe (III) hydrogel. This study obtained the maximum adsorption capacity of 294.5 mg g<sup>-1</sup> in 10 mL at a dosage of 0.02 g, a pH of 12, and 25 °C with a concentration of 50 mg L<sup>-1</sup><sup>33</sup>.

Nowadays, design of experiments (DOEs) such as response surface methodology (RSM) are used instead of classical methods (one-factor-at-a-time)<sup>34</sup>. RSM is a combination of mathematical and statistical methods used in process optimization, where many variables affect the desired response. This method can be performed to lower the number of tests, determine square regression coefficients, and evaluate the relationship between one or more responses using the influence of independent variables<sup>35,36</sup>.

Therefore, the present study aims to investigate the efficiency of Fe<sub>3</sub>O<sub>4</sub>/CS adsorbent to remove TMP and SMX from aqueous solutions. Further, the effect of pH, sonication time, adsorbent amount, and analyte concentration on the removal efficiency of contaminants is investigated. Analysis of variance (ANOVA) was used as a statistical method to analyze the responses. Moreover, BBD-based RSM was employed to achieve appropriate response levels for optimizing the removal of contaminants from aqueous solutions. Overall, this design has several advantages, such as reducing the number of tests, time, and cost and increasing removal efficiency.

## Materials and method

**Reagents and materials.** All chemicals used in the experiments were of analytical grade. Chitosan was purchased from Aladdin Chemical Reagent Co. Ltd. Also, Iron (II) chloride, tetrahydrate, iron (III) chloride hexahydrate, trimethoprim, sulfamethoxazole, ethanol, acetone, hydrochloric acid, ammonia, acetic acid, sodium hydroxide, acetonitrile, and nitric acid were obtained from Sigma Aldrich Co. Ltd. Distilled water was used in all experiments to increase the volume of the solutions. The stock solution was prepared from each antibiotic with a concentration of 1000 mg L<sup>-1</sup>, and pH was determined via a pH-Meter. The ultrasonic bath was used to create interaction between the adsorbent and analyte. The samples containing antibiotics were analyzed by UV-Vis spectrophotometer. A centrifuge and a magnet were also used to separate the adsorbent from the solution. Adsorbent characteristics such as morphology, adsorbent shape, and phase characteristics were investigated using scanning electron microscopy (SEM), transmission electron microscopy (TEM), X-ray diffraction (XRD), pH of zero point of charge (pH<sub>ZPC</sub>), vibrating sample magnetometer (VSM), and Fourier-transform infrared (FTIR).

**Synthesis of Fe<sub>3</sub>O<sub>4</sub> NPs.** Fe<sub>3</sub>O<sub>4</sub> NPs were synthesized by the co-precipitation method. To this end, a mixture of 4 mL FeCl<sub>3</sub> (2 M) and 2 mL FeCl<sub>2</sub> (2 M) was prepared in a flat-bottom beaker. This solution was severely stirred for 30 min at 30 °C, and chemical precipitation was formed by slowly adding 100 mL of ammonia solution (1 M) to the mixture. The steps for this process were carried out under intense stirring and N<sub>2</sub> gas. Black Fe<sub>3</sub>O<sub>4</sub> NPs were separated by an external magnet. Finally, the NPs were rinsed with distilled water and ethanol until the pH reached 7.

**Synthesis of Fe<sub>3</sub>O<sub>4</sub>/CS NPs.** Fe<sub>3</sub>O<sub>4</sub>/CS NPs were prepared using the co-precipitation method. To this end, 0.3 g of chitosan was dissolved in 50 mL of acetic acid solution (1%, V/V). Then, 2 g of Fe<sub>3</sub>O<sub>4</sub> NPs prepared in the previous section were added to the mixture. The mixture was stirred for 30 min, followed by adding 50 mL

of 1 M NaOH solution to the suspension to obtain Fe<sub>3</sub>O<sub>4</sub>/CS NPs. Finally, the prepared NPs were rinsed with distilled water until the pH reached 7 and then dried. The properties and morphology of the Fe<sub>3</sub>O<sub>4</sub>/CS NPs were investigated using SEM, VSM, p*H*<sub>zpc</sub>, TEM, FTIR, and XRD analyses.

**pH of zero point of charge (p*H*<sub>zpc</sub>).** The p*H*<sub>zpc</sub> is the point at which the surface charge of the adsorbent is neutral. It is one of the crucial stages in determining the surface characteristics of the adsorbent. For this purpose, 10 Erlenmeyer flasks (100 mL) containing 30 mL of NaCl solution (0.01 M) were prepared, and each Erlenmeyer flask was adjusted to different pH values ranging from 2 to 11. The pH adjustments were performed using NaOH (0.1 M) and HCl (0.1 M). Subsequently, 0.2 g of the adsorbent was added to each Erlenmeyer, and the Erlenmeyers were placed on a shaker for 24 h. After 24 h and the separation of the adsorbent from the solution, the final pH was measured. The difference between the initial and final pH values was calculated, and the ΔpH curve was plotted against the initial pH values. The point where the curve intersects the X-axis is called the p*H*<sub>zpc</sub>.

**Response surface methodology (RSM).** RSM applies experimental techniques to design and optimize the relationships between the test factors. Next, after checking the responses, it analyzes and presents graphs based on one or more criteria<sup>37</sup>. In this research, pH solution (A), analyte concentration (B), adsorbent amount (C), and sonication time (D) were selected as parameters affecting the removal performance of antibiotics. Design-Expert® software (version 10) was used to examine the effect of parameters on response performance (removal efficiency). Then, experiments were designed using Box–Behnken Design. The number of experiments was determined using Eq. (1).

$$N = 2K(K - 1) + C_o \quad (1)$$

where *K* is the number of investigated parameters and *C*<sub>o</sub> is the number of repetitions of the experiment steps<sup>38</sup>.

A total of 29 experiments (with 5 central replicates) were designed and implemented for each analyte. After selecting the model, the equation of the model and its predicted coefficients were determined through the quadratic equation (Eq. 2):

$$Y = \beta_0 + \sum_{i=1}^k \beta_i X_i + \sum_{i=1}^k \beta_{ii} X_i^2 + \sum_{i \leq j}^k \sum_j^k \beta_{ij} X_i X_j \quad (2)$$

where,  $\beta_0$ ,  $\beta_i$ ,  $\beta_{ii}$ , and  $\beta_{ij}$  are constant, linear, quadratic, and interaction coefficients of regression, respectively. Also,  $X_i$  and  $X_j$  denote coded independent variables, and *k* is the number of variables<sup>39</sup>. Statistical analysis was run to evaluate the accuracy and adequacy of the model using ANOVA, with probability values of Prob < *F* > 0.05. Further, the predictability and adequacy of the model were tested using the coefficient of determination of linear regression (*R*<sup>2</sup>), adequate precision, the lack of fit criterion, adjusted determination coefficient (Adj-*R*<sup>2</sup>), and detect the residuals. For the experimental design in the current study, four factors were selected, including pH, adsorbent amount, antibiotic concentration, and sonication time. Each factor was considered at three levels, as shown in Table 1.

**Adsorption experiments.** All adsorption experiments were done in a discontinuous system. For this purpose, 100 mL of solutions containing different concentrations of antibiotics were prepared in 250 mL Erlenmeyer flasks. Moreover, pH in the range of 3 to 9 was investigated to examine the effect of pH on the removal of analytes. Then, 0.05–0.15 g of Fe<sub>3</sub>O<sub>4</sub>/CS NPs was added to the solutions containing the analytes. The solutions prepared based on the model provided by RSM were placed in the ultrasonic bath, and the time was determined for each test by the software. Afterward, the adsorbent was separated from the sample using centrifugation and an external magnetic field. In the next step, the concentration of antibiotics was measured by UV–Vis spectrophotometer. Finally, the removal efficiency was calculated using Eq. (3).

$$\%R = \frac{C_o - C_e}{C_o} \times 100 \quad (3)$$

In this equation, *C*<sub>o</sub> (mg L<sup>-1</sup>) was the initial concentration of the analyte in the solution, *C*<sub>e</sub> (mg L<sup>-1</sup>) was the equilibrium concentration of the analyte after the equilibration time, and *R* was the removal efficiency<sup>40</sup>.

Variables	Symbol	Unit	Range and levels		
			- 1	0	+ 1
pH of the solution	A	-	3	6	9
Analyte concentration	B	mg L <sup>-1</sup>	10	20	30
Adsorbent amount	C	g	0.05	0.10	0.15
Sonication time	D	min	10	20	30

**Table 1.** The BBD based on RSM.

## Results and discussion

**Characterization of  $\text{Fe}_3\text{O}_4/\text{CS}$  NPs.** SEM images were captured for the  $\text{Fe}_3\text{O}_4/\text{CS}$  sample to examine the size of nanoparticles and their morphology (Fig. 1A). Figure 1A shows a spherical morphology and uniformity for the sample, along with appropriate granulation with no aggregation. In addition, particle size was determined between 75 and 81 nm. Figure 1B illustrates the TEM image of  $\text{Fe}_3\text{O}_4/\text{CS}$  adsorbent. The TEM image in Fig. 1B confirms the sample's spherical morphology and uniform size. Moreover, the magnetic property of the synthesized  $\text{Fe}_3\text{O}_4/\text{CS}$  sample was tested by the VSM method at room temperature (Fig. 1C). The magnetic diagram for the sample is similar to the letter S, and the curved shape of the sample confirms the superparamagnetic property of the sample. In addition, the degree of saturation of the sample was equal to  $25 \text{ emu g}^{-1}$ . This value suggests the high magnetic property of the sample and its easy separation from the reaction environment by an external magnet. The magnetic property of the sample was compared by performing VSM analysis for the pure iron oxide nanoparticles. For the pure  $\text{Fe}_3\text{O}_4$  sample, the saturation magnetization was  $59 \text{ emu g}^{-1}$ , which is much

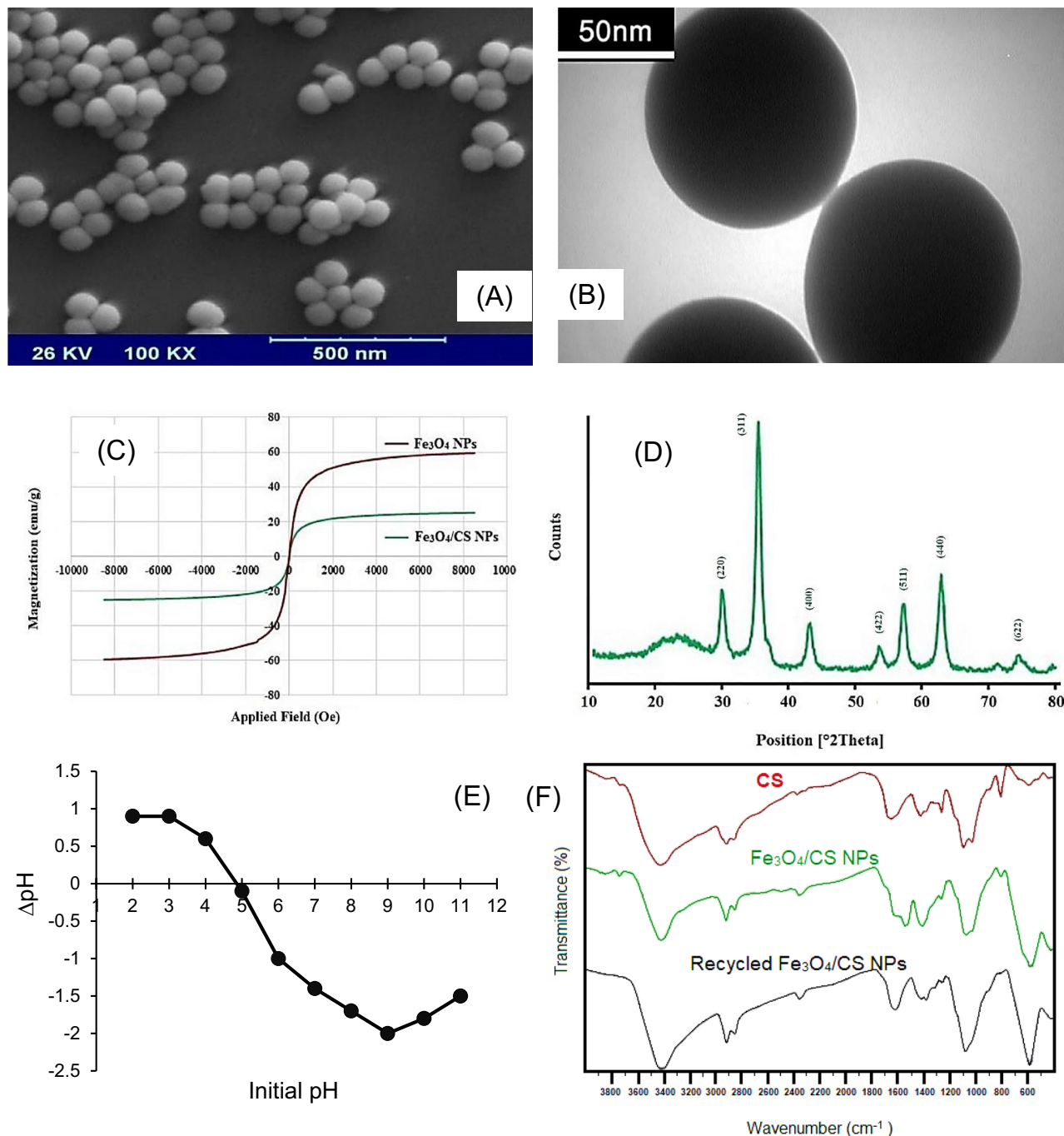


**Figure 1.** (A) SEM image, (B) TEM image, (C) VSM magnetization curve, (D) XRD pattern, (E)  $\text{pH}_{\text{zpc}}$  and (F) FTIR analysis of  $\text{Fe}_3\text{O}_4/\text{CS}$  NPs adsorbent and after 6 cycles of sorption desorption processes.

higher than that of the Fe<sub>3</sub>O<sub>4</sub>/CS composite sample. This result indicates the presence of chitosan next to iron oxide nanoparticles and the change of iron percentage in the sample compared to its pure ratio. XRD analysis was performed to identify and confirm the structure of Fe<sub>3</sub>O<sub>4</sub>/CS crystals. For the Fe<sub>3</sub>O<sub>4</sub>/CS sample, the position and relative intensity of all peaks according to the standard XRD pattern for Fe<sub>3</sub>O<sub>4</sub> NPs is JCPDS card no. 1436-85<sup>41</sup>. The presence of sharp peaks with high intensity indicates a good network structure. On the other hand, the absence of additional peaks confirms the purity and the absence of impurities in the produced sample (Fig. 1D). Seven peaks with angles of 30.2°, 35.8°, 43.5°, 53.7°, 57.4°, 62.8°, and 75.3° and corresponding crystal planes of 220, 311, 400, 422, 511, 440, and 622, respectively, were identified in the spectrum. These peaks are related to iron oxide nanoparticles with a cubic spinel lattice structure. Moreover, the weak broad peak that appeared at the angle of 21–28 is related to chitosan, which is present in the substrate of the magnetic composite sample. The size of Fe<sub>3</sub>O<sub>4</sub>/CS crystals was about 70 nm using the Debye–Scherrer Equation. The results of pH determination showed that the Fe<sub>3</sub>O<sub>4</sub>/CS adsorbent surface has zero electric charge at pH = 4.9 (Fig. 1E). Therefore, the adsorbent surface will have a positive electrical charge at a pH lower than p*H*<sub>zpc</sub> and a negative electrical charge at a pH higher than p*H*<sub>zpc</sub>. FTIR spectroscopy was used to identify and confirm the structure of Fe<sub>3</sub>O<sub>4</sub>/CS NPs. For this purpose, FT-IR analysis was carried out from two combinations of Fe<sub>3</sub>O<sub>4</sub>/CS NPs, CS. Besides, FT-IR analysis of Fe<sub>3</sub>O<sub>4</sub>/CS NPs was also performed after 6 cycles of sorption and desorption. In the FT-IR spectrum related to chitosan, the broad peak at 3427 cm<sup>-1</sup> is related to the stretching vibrations of amine and hydroxyl groups on the chitosan chain, and the peaks at 2922 cm<sup>-1</sup> and 2851 cm<sup>-1</sup> are attributed to the stretching vibrations of carbon–hydrogen bonds. The bending vibrations related to the nitrogen–hydrogen bond appear at 1649 cm<sup>-1</sup> and the peak at 1262 cm<sup>-1</sup> is related to the carbon–oxygen stretching of the first type of alcohol in the chitosan chain. The double peaks at 1093 cm<sup>-1</sup> and 1027 cm<sup>-1</sup> are attributed to the carbon–oxygen stretching vibrations of the chitosan structure. The FT-IR analysis of Fe<sub>3</sub>O<sub>4</sub>/CS NPs shows well all the peaks related to chitosan with a slight shift, in addition to the sharp and distinct peak at 576 cm<sup>-1</sup> related to the stretching vibration of the iron–oxygen (Fe–O) bond, which is added to it. It confirms the presence of iron oxide nanoparticles in the composition. Also, as shown in Fig. 1F, these peaks were again observed with full intensities like the initial absorbance when performing the desorption processes.

**Statistical analysis.** Design Expert software was used for regression analysis, drawing RSM graphs, and ANOVA. ANOVA results are presented in Tables 2 and 3. The tables show the parameters and statistical analysis of the presented second-order model for removing TMP and SMX. The determination coefficient (R<sup>2</sup>) and adjusted determination coefficient (Adj-R<sup>2</sup>) were used to estimate the goodness of the fit of the model. The high value of R<sup>2</sup> (i.e., 0.9993 for TMP and 0.9973 for SMX) indicates that the model can explain more than 99.7% of the variation. Also, the value of Adj-R<sup>2</sup> more than 0.99 shows a high degree of correlation between the experimental and predicted values. Therefore, the closer the R<sup>2</sup> and Adj-R<sup>2</sup> are to 1, the better the model describes response changes as a function of independent variables. The significance of the model for removing the contaminants is expressed by F-value, which was 1433.03 and 373.25 for TMP and SMX, respectively. Adeq-Precision shows the difference between the model's predicted response and the average value of the prediction error. When this criterion is greater than 4, it indicates the acceptable discrimination power of the model. In this

Source	Sum of squares	DF	Mean square	F-value	p-value	
Model	13,732.60	14	980.90	1433.03	<0.0001	Significant
A	851.77	1	851.77	1244.37	<0.0001	
B	25.87	1	25.87	37.80	<0.0001	
C	117.31	1	117.31	171.39	<0.0001	
D	212.69	1	212.69	310.72	<0.0001	
A*B	188.93	1	188.93	276.01	<0.0001	
A*C	2469.59	1	2469.59	3607.90	<0.0001	
A*D	4.16	1	4.16	6.08	0.0272	
B*C	1083.73	1	1083.73	1583.25	<0.0001	
B*D	577.20	1	577.20	843.25	<0.0001	
C*D	220.67	1	220.67	322.38	<0.0001	
A <sup>2</sup>	4098.83	1	4098.83	5988.09	<0.0001	
B <sup>2</sup>	4228.65	1	4228.65	6177.76	<0.0001	
C <sup>2</sup>	21.85	1	21.85	31.91	<0.0001	
D <sup>2</sup>	1931.29	1	1931.29	2821.48	<0.0001	
Residual	9.58	14	0.68			
Lack of fit	4.49	10	0.45	0.35	0.9175	Not significant
Pure error	5.09	4	1.27			
Cor total	13,742.19	28				
R <sup>2</sup> = 0.9993	R <sup>2</sup> adjust = 0.9986		Adeq-precision = 113.73			

**Table 2.** ANOVA for response surface quadratic model for removal of TMP. DF degree of freedom.



Source	Sum of squares	DF	Mean square	F-value	p-value	
Model	6545.06	14	467.50	373.25	<0.0001	Significant
A	140.43	1	140.43	112.11	<0.0001	
B	74.25	1	74.25	59.28	<0.0001	
C	538.01	1	538.01	429.54	<0.0001	
D	338.03	1	338.03	269.88	<0.0001	
A*B	16.40	1	16.40	13.10	0.0028	
A*C	1260.61	1	1260.61	1006.44	<0.0001	
A*D	52.13	1	52.13	41.62	<0.0001	
B*C	383.38	1	383.38	306.08	<0.0001	
B*D	65.85	1	65.85	52.58	<0.0001	
C*D	13.69	1	13.69	10.93	0.0052	
A <sup>2</sup>	2295.41	1	2295.41	1832.61	<0.0001	
B <sup>2</sup>	1609.38	1	1609.38	1284.90	<0.0001	
C <sup>2</sup>	243.67	1	243.67	194.54	<0.0001	
D <sup>2</sup>	1059.28	1	1059.28	845.71	<0.0001	
Residual	17.54	14	1.25			
Lack of fit	11.94	10	1.19	0.85	0.6200	Not significant
Pure error	5.59	4	1.40			
Cor total	6562.59	28				
R <sup>2</sup> = 0.9973	R <sup>2</sup> Adjust = 0.9947		Adeq-Precision = 65.61			

**Table 3.** ANOVA for response surface quadratic model for removal of SMX. *DF* Degree of freedom.

study, Adeq-Precision for removing TMP and SMX was 113.73 and 65.61, respectively. Another parameter used to evaluate the model is the lack of fit (LOF) test. This test is significant if the *P*-value of the model is greater than 0.05 (95% significance level). Tables 2 and 3 show that the *P*-value for removing TMP and SMX is greater than 0.05. Quadratic equations (Eqs. 4 and 5) demonstrate the mathematical relationship between the parameters for removing TMP and SMX using RSM.

$$\begin{aligned} \% \text{Removal-TMP} = & +88.23 + 8.42 * A - 1.46 * B + 3.12 * C \\ & - 4.21 * D - 6.87 * A * B - 24.84 * A * C - 1.02 * A * D \\ & + 16.46 * B * C - 12.01 * B * D - 7.42 * C * D - 25.13 * A^2 \\ & - 25.53 * B^2 - 1.83 * C^2 - 17.25 * D^2 \end{aligned} \quad (4)$$

$$\begin{aligned} \% \text{Removal-SMX} = & +93.14 + 3.42 * A - 2.48 * B + 6.69 * C \\ & - 5.30 * D - 2.02 * A * B - 17.75 * A * C + 3.61 * A * D \\ & + 9.79 * B * C - 4.05 * B * D - 1.85 * C * D - 18.81 * A^2 \\ & - 15.75 * B^2 - 6.12 * C^2 - 12.77 * D^2 \end{aligned} \quad (5)$$

The positive sign in front of the parameters displays the synergistic effect of the variable on the model. Meanwhile, the negative sign indicates a decreasing or opposite effect on the model. When an increase in the value of one variable is followed by an increase in the value of another variable, a positive correlation coefficient is obtained, which indicates synergy. On the other hand, when a reduction in the value of one variable is followed by a reduction in another variable, a negative correlation coefficient is obtained, indicating disintegration. Table 4 presents the experimental results and the results obtained from the Design-Expert<sup>®</sup> software for removing TMP and SMX.

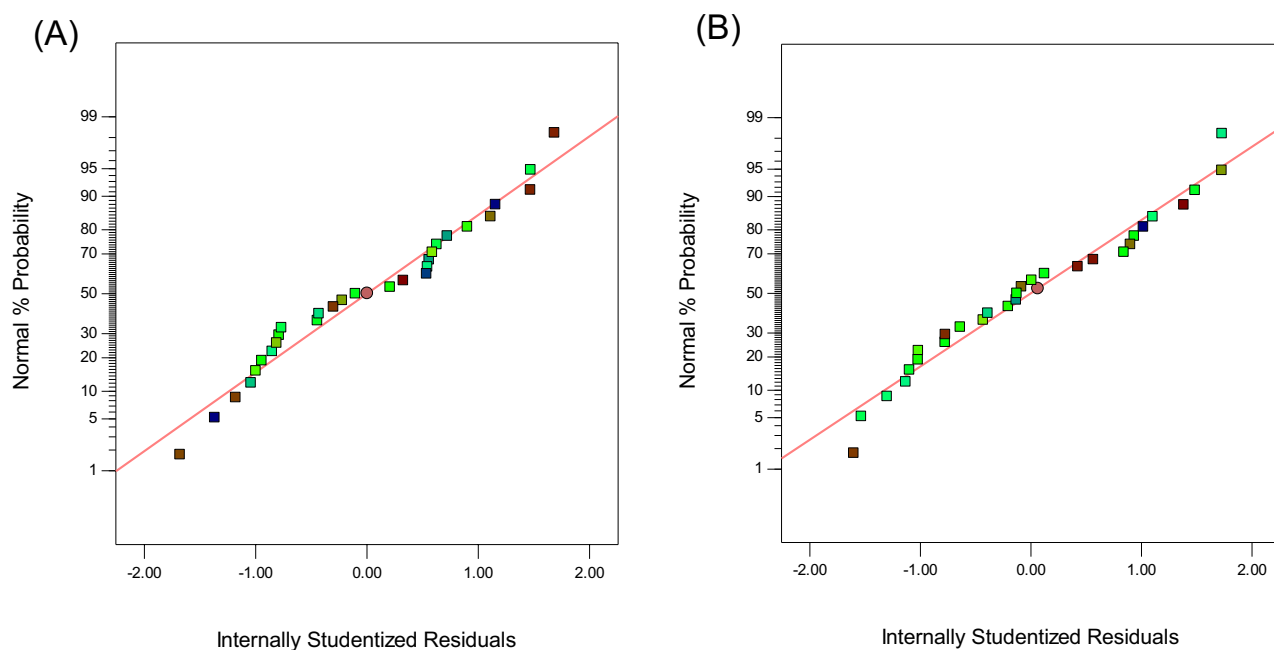
In addition to the mentioned criteria to evaluate the model's accuracy, the difference between the experimental and predicted residuals was used to test the model's accuracy (Figs. 2, 3, 4). The residuals are considered unfit changes by the model. Figure 2A and B present the residual diagram for evaluating the normal distribution of the residuals. The points in the normal graph of the residuals form a straight line, confirming the normal distribution of residuals.

Figure 3A and B display the actual versus predicted values for each model. The response values against the actual values are presented to help identify values or groups of values not predicted by the model. According to Fig. 3A and B, there is a trivial difference between predicted values and the experimental results.

Figure 4A and B provide Box-Cox curves. This figure is a tool to identify the most appropriate power transfer function to be applied to the response. The lowest point in the Box-Cox graph reflects the best Lambda value (Lambda: the minimum residual sum of squares in the transformed model). This figure also illustrates a 95% confidence interval. According to the Box-Cox graph, the value of Lambda was considered equal to 1, and no transformation was needed. The graphs related to the adequacy of the model also exhibit the good performance of the model.

Run	Variables				%Removal-TMP		%Removal-SMX	
	A	B	C	D	Experimental	Predicted	Experimental	Predicted
1	0	-1	-1	0	75.98	75.67	76.11	76.84
2	0	0	1	1	60.21	60.63	73.78	73.77
3	-1	1	0	0	34.84	34.54	53.88	54.70
4	0	1	1	0	78.55	78.98	86.51	85.26
5	1	0	-1	0	91.58	91.40	82.37	82.68
6	0	0	-1	1	68.70	69.23	63.29	64.08
7	0	1	-1	0	40.10	39.81	53.54	52.29
8	-1	0	-1	0	24.13	24.86	41.07	40.33
9	0	0	0	0	89.48	88.23	92.37	93.14
10	-1	0	0	-1	40.15	40.60	66.49	67.05
11	1	-1	0	0	54.09	54.33	67.19	66.51
12	1	0	1	0	48.75	47.96	59.46	60.57
13	0	0	0	0	87.36	88.23	93.71	93.14
14	0	0	-1	-1	63.28	62.80	70.85	71.00
15	1	0	0	-1	58.99	59.49	67.28	66.67
16	1	1	0	0	37.09	37.65	56.55	57.49
17	-1	0	0	1	34.61	34.22	49.12	49.21
18	0	0	0	0	88.01	88.23	94.53	93.14
19	0	0	1	-1	84.50	83.91	88.74	88.09
20	0	0	0	0	86.99	88.23	93.57	93.14
21	0	1	0	-1	60.31	60.20	71.03	71.49
22	0	-1	0	1	54.66	54.72	65.94	65.85
23	0	-1	0	-1	38.88	39.11	68.26	68.35
24	0	-1	1	0	48.59	49.00	69.92	70.66
25	0	1	0	1	28.04	27.75	52.48	52.76
26	1	0	0	1	49.37	49.03	64.35	63.28
27	0	0	0	0	89.32	88.23	91.54	93.14
28	-1	0	1	0	80.69	80.81	89.17	89.23
29	-1	-1	0	0	24.35	23.73	56.42	55.62

**Table 4.** BBD matrix for removal of TMP and SMX.



**Figure 2.** Normal plot of residuals for (A) TMP and (B) SMX.

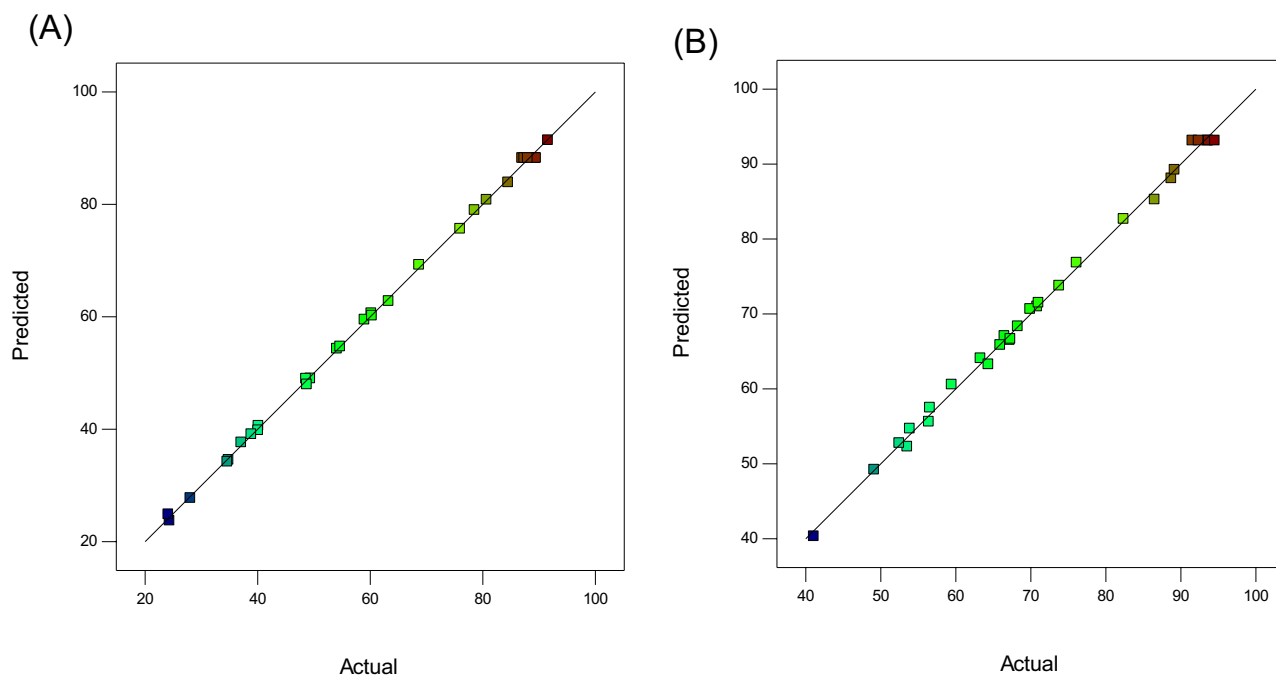


**Figure 3.** Graph of actual values versus predicted values for (A) TMP and (B) SMX.

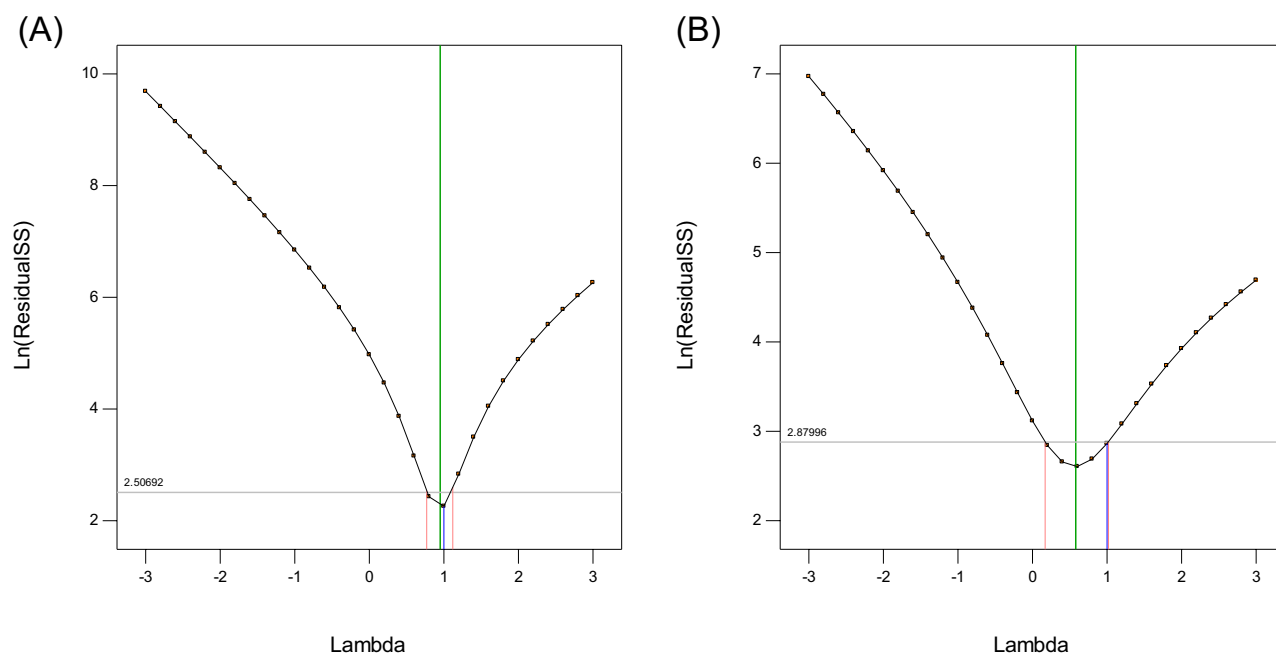


**Figure 4.** Box-Cox curve for (A) TMP and (B) SMX.

**Three-dimensional.** The effect of changes in TMP concentration on TMP removal efficiency in optimal conditions (pH of 6, adsorbent amount of 0.13 g/100 mL, and sonication time of 15 min) is presented in Fig. 5A. Changes in TMP concentration were investigated in the range of 10 to 30 mg L<sup>-1</sup>. The results (Fig. 5A) indicated that by keeping other factors (e.g., sonication time, adsorbent amount, and pH) constant in optimal conditions, the amount of TMP ion removal reduced with increasing concentration. As a result, the highest removal efficiency was observed at a concentration of 22 mg L<sup>-1</sup>. The explanation is that with the increase in the concentration of antibiotics in the solution, the competition for access to the binding sites from the adsorbent increases, and all the binding sites are exposed to analytes. Finally, it can be concluded that with the increase in concentration, the adsorbent surface is quickly saturated, and the removal percentage decrease. In other words, at low concentrations, more effective adsorption sites are available for antibiotics. In contrast, at higher concentrations, the number of antibiotics is much higher than that of adsorption sites on the adsorbent. Hence, the adsorption



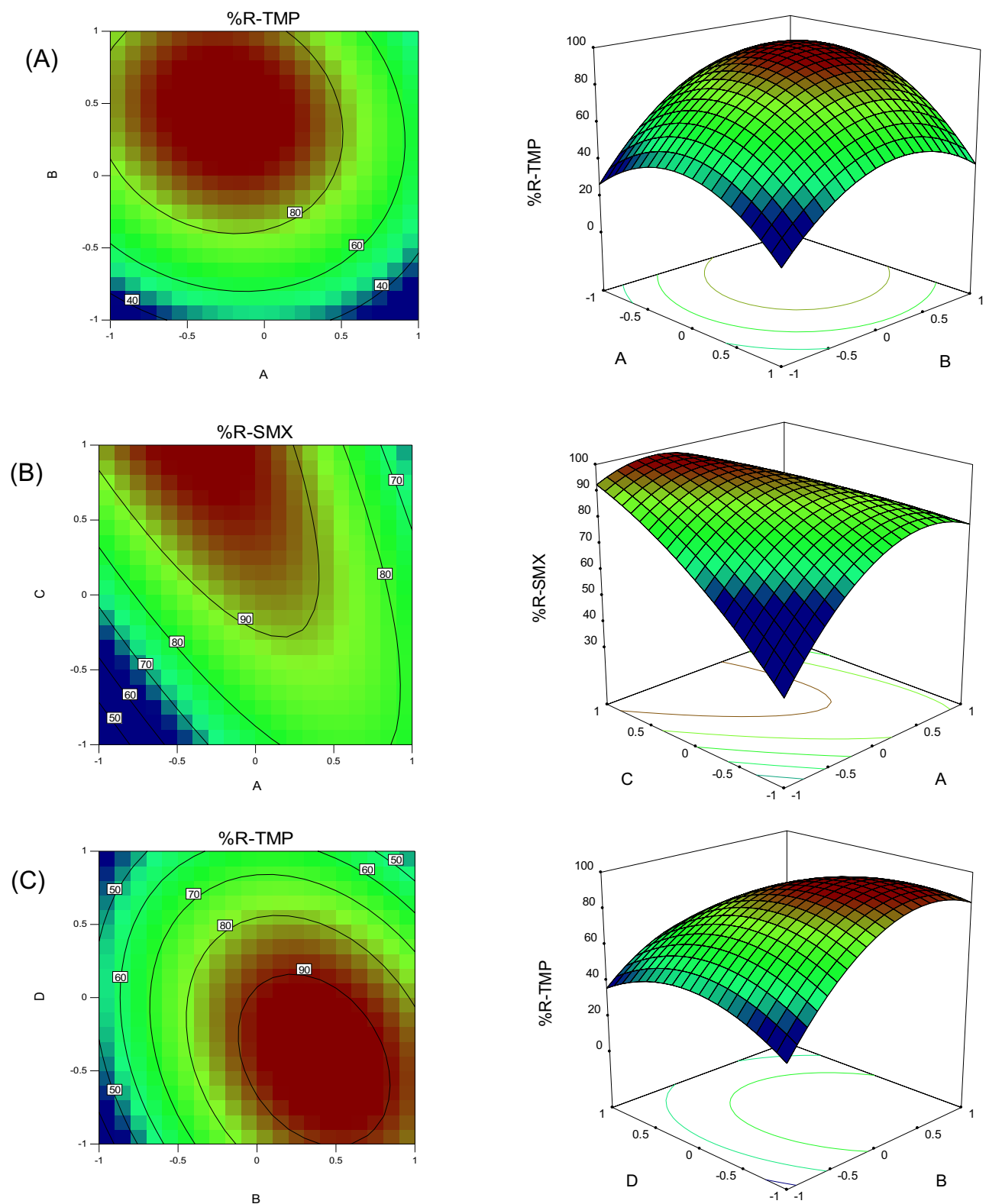


**Figure 5.** The three-dimensional (3D) plots of removal of (A) TMP, (B) SMX, and (C) TMP.

of cations depends on the initial concentration, and with increasing concentration, the absorption percentage decreases. Norzaee et al. investigated the removal of penicillin G antibiotics via persulfate. The results proved that the removal efficiency decreases with the increase in the initial concentration of antibiotics<sup>42</sup>. Similar results were obtained by Gao et al. on removing antibiotics from industrial wastewater by graphene oxide<sup>43</sup>.

Figure 5A illustrates the effect of pH on the removal efficiency of TMP by the adsorbent. The percentage of TMP removal increased as the pH changed from 3 to 6. Subsequently, at higher pH values, the removal of antibiotics decreased. The  $pH_{zpc}$  of  $Fe_3O_4/CS$  adsorbent was calculated to be 4.9. At pH values above the  $pH_{zpc}$ , the surface of  $Fe_3O_4/CS$  adsorbent becomes negatively charged due to the presence of hydroxide ions ( $OH^-$ ), enabling the adsorption of antibiotics. The maximum removal for TMP and SMX was observed at  $pH = 6$ . It was assumed that at  $pH < 6$ , the high hydronium ions ( $H_3O^+$ ) concentration competes with antibiotics, leading to reduced adsorption at lower pH levels. When the pH value was  $> 6$ , the increase in alkaline conditions and  $OH^-$  concentration in the solution resulted in electrostatic repulsion. Therefore, the removal efficiency decreased at higher pH values due to electrostatic repulsion. Wang and You investigated the removal of antibiotics from aqueous environments by iron oxide/activated carbon nanoparticle composite. The results showed that the removal rate of antibiotics is extremely low at a pH of less than 6. They explained this result by the high concentration of  $H^+$  ions in the experiment environment. These ions occupy the binding sites on the adsorbent surface and exhibit greater competition for surface adsorption<sup>44</sup>.

Figure 5B depicts the simultaneous effect of the two parameters (i.e., adsorbent amount and pH) on SMX removal. The results in Fig. 5B suggest that the analyte removal percentage increases with increasing the adsorbent amount. This outcome can be due to the rise in empty and unoccupied sites with increasing adsorbent content. In general, the surface adsorption of analytes increases with increasing the adsorbent since more adsorption sites will be available. When the amount of adsorbent is low, the removal percentage reduces, probably due to insufficient active sites and saturation of the adsorbent surface. In a study, Yang et al., using graphene oxide as an adsorbent to remove antibiotics from aqueous solutions, yielded results similar to those of the present research. Their results indicated that the removal efficiency increases with increasing the adsorbent amount<sup>45</sup>.

Figure 5C provides the effect of TMP concentration and reaction time on TMP removal efficiency. According to Fig. 5C, the removal efficiency increases by increasing the reaction time. The reason is that with the accumulation of analyte molecules in empty and unoccupied sites over time, the analyte concentration reduces, and the removal rate increases. Askari et al. investigated the removal of antibiotics from aqueous environments using walnut wood and magnetized with cobalt ferrite. The results revealed that the increase in time caused an increase in the removal percentage of antibiotics<sup>46</sup>. Similar results were obtained regarding the increase in removal percentage with increasing contact time in studies by Lanjwani et al., Vu et al., and Mohammed et al.<sup>47–49</sup>.

**Optimal points.** The optimal points for removing the contaminants were obtained using the Design-Expert software, as reported in Table 5. The optimization is performed to find points with a higher removal index. This study optimized the important factors in removal efficiency (i.e., adsorbent amount, antibiotics concentration, sonication time, and pH solution). Table 5 represents the optimization results. It is of note that the experiments were done under optimal conditions to confirm the results obtained from the model prediction. The results indicated a good agreement with the removal value predicted by the model under optimal conditions.

**Desorption studies.** The desorption of the analyte from the adsorbent surface for its reuse is crucial. The desorption experiments of antibiotics from the  $Fe_3O_4/CS$  NPs surface were carried out using various solvents such as acetonitrile, acetone, ethanol, and nitric acid. These experiments were conducted under optimal conditions for the variables. After separating  $Fe_3O_4/CS$  NPs using an external magnetic field, the adsorbent surface was washed with the desired solvent. Finally, the remaining antibiotic concentration was measured using a UV/Vis spectrophotometer. Among four different solvents (ethanol, acetone, nitric acid, and acetonitrile), ethanol showed the highest desorption for TMP and SMX from the  $Fe_3O_4/CS$  NPs (Fig. 6). Therefore, ethanol was selected as the solvent in subsequent experiments.

**Reusability of  $Fe_3O_4/CS$  NPs.** The expanded process of desorption has been adopted to reduce the production costs of the adsorbent and minimize the remaining waste materials. Based on the results, ethanol was selected as the most efficient solvent for the desorption of TMP and SMX from the adsorbent surface. Therefore, after the absorption of TMP and SMX from the aqueous solution with  $Fe_3O_4/CS$  NPs, the adsorbent was recovered and reused through six consecutive cycles of desorption with ethanol. Figure 7 illustrates the efficiency of desorption over the six stages of the recovery process. According to the results, the recovery percentage for TMP and SMX only decreased by about 5% after five cycles of absorption and desorption, indicating more than 95% recovery. The acceptable reduction in adsorption capacity signifies the remarkable stability of the adsorbent and the non-degradation of the  $Fe_3O_4/CS$  NPs structure, which highlights the economic feasibility of synthesizing and utilizing this adsorbent for the treatment of wastewater containing TMP and SMX. Figure 7C depicts the method of separating  $Fe_3O_4/CS$  NPs from the sample medium.

Run	A	B	C	D	%Removal-TMP		%Removal-SMX	
					Experimental	Predicted	Experimental	Predicted
1	6	22	0.13	15	93.85	93.51	95.98	97.14
2	6	22	0.13	15	93.40	93.51	97.24	97.14
3	6	22	0.13	15	92.46	93.51	98.01	97.14

**Table 5.** Optimum conditions of removal of TMP and SMX.

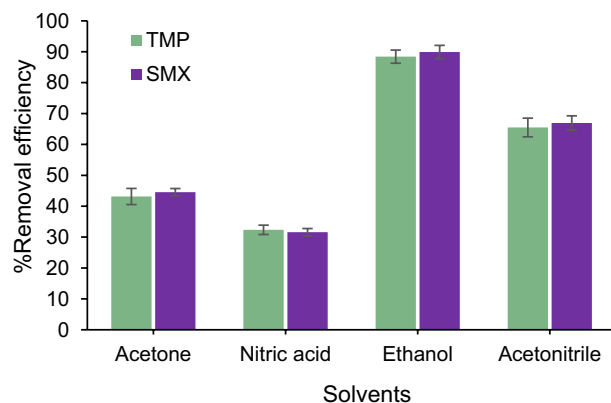


**Figure 6.** The effect of solvent on the desorption of analyte.

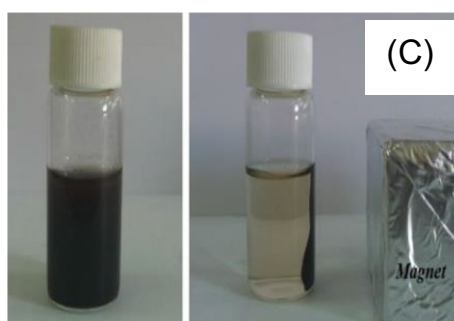
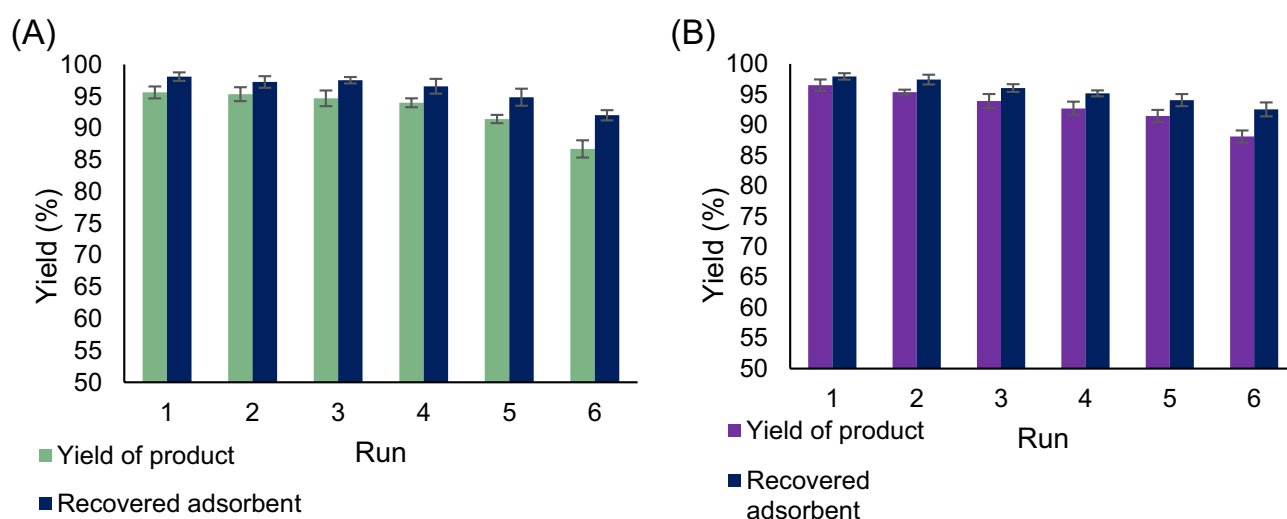


**Figure 7.** The reusability of adsorbent for removal of (A) TMP, (B) SMX, and (C) the removal illustration.

**Analysis of real samples.** Several water samples (i.e., tap water, wastewater, and lake water fish farm) were used to test the validity and applicability of the proposed method. Then, TMP and SMX removal experiments were carried out on real samples under optimal conditions. To this end, water samples were filtered to remove suspended particles, and then experiments were performed according to the method stated in “Synthesis of  $\text{Fe}_3\text{O}_4/\text{CS NPs}$ ” section. According to the results (Table 6), the removal efficiency of TMP and SMX in environmental water samples was in the range of 91.23%–98.28%, indicating that the sample texture has a trivial effect on the efficiency of the method.

**Comparison with other methods.** The performance comparison of the proposed adsorbent with other adsorbents is shown in Table 7. The results of Table 7 showed that the proposed method was comparable to other methods available in the literature. On the other hand, the contact time for our research was superior to other adsorbents for removing TMP and SMX. The results showed that the ultrasonic-assisted removal method

Real samples	%Removal-TMP $\pm$ RSD	%Removal-SMX $\pm$ RSD
Tap water	93.57 $\pm$ 2.07	95.14 $\pm$ 1.52
Fish farm	91.89 $\pm$ 3.09	91.23 $\pm$ 2.02
Wastewater	92.58 $\pm$ 2.30	95.20 $\pm$ 2.76
Lake water	95.95 $\pm$ 1.66	93.42 $\pm$ 1.80

**Table 6.** Results of removal of TMP and SMX in real samples (n = 3).

Adsorbent	Analyte	Concentration (mg L <sup>-1</sup> )	Adsorbent amount	pH	Time	Adsorption capacity or %removal	Ref
Activated carbon F400	TMP	10	50 mg	7	30 min	70.6%	50
Granular activated carbon	SMX	25	4 g	7	100 min	94.23%	51
Amberlite XAD-7	TMP	50	3 g	7	120 min	70%	52
Hierarchical magnetic zinc oxide-based composite ZnO@g-C <sub>3</sub> N <sub>4</sub>	SMX	30	0.65 g	5.6	60 min	90.4%	53
Vegetal powdered activated carbon	TMP	15	100 mg	6	30 min	135 mg g <sup>-1</sup>	54
Fe-MIL-88B-NH <sub>2</sub> carbonaceous nanocomposites	SMX	100	25 mg	6	12 h	73.53 mg g <sup>-1</sup>	55
Fe <sub>3</sub> O <sub>4</sub> /CS NPs	TMP	22	0.13 g	6	15 min	95.60%	This study
Fe <sub>3</sub> O <sub>4</sub> /CS NPs	SMX	22	0.13 g	6	15 min	95.16%	This study

**Table 7.** Literature comparison of removal for TMP and SMX.

significantly improves the efficiency of the removal. Also, using the optimization method with the help of RSM reduces the number of tests and the consumption of materials.

## Conclusions

The present study used Fe<sub>3</sub>O<sub>4</sub>/CS NPs to determine the removal process of TMP and SMX. Accordingly, BBD-based RSM was applied to evaluate the effect of parameters on response performance. Independent variables, such as pH, sonication time, adsorbent amount, and analyte concentration, were optimized in removing TMP and SMX. The results of SEM, VSM, XRD, and TEM showed that the Fe<sub>3</sub>O<sub>4</sub>/CS NPs were successfully prepared and existed as spherical nanoparticles with an average size of about 70 nm. The large R<sup>2</sup> coefficient guarantees the fit of the quadratic model and indicates good processing of the data under investigation. After optimization, the removal amount of TMP and SMX at a pH of 6, concentration of 22 mg L<sup>-1</sup>, adsorbent amount of 0.13 g/100 mL, and contact time of 15 min was 93.85% and 98.01%, respectively. The results of desorption studies showed that ethanol as a solvent increased the desorption efficiency of antibiotics from the adsorbent surface. Furthermore, reusability showed that Fe<sub>3</sub>O<sub>4</sub>/CS NPs could be used up to 6 times efficiently to remove TMP and SMX. The results also suggested that Fe<sub>3</sub>O<sub>4</sub>/CS NPs effectively removed TMP and SMX from real water samples and can remove TMP and SMX in the range of 91.23% to 95.95%. The results of real water samples analysis showed that the sample matrix had no significant effect on removing the TMP and SMX antibiotics from water samples. The experimental results demonstrated that Fe<sub>3</sub>O<sub>4</sub>/CS NPs could be employed successfully as environmentally friendly adsorbents for removing TMP and SMX antibiotics from the water samples.

## Data availability

The datasets used and/or analyzed during the current study are available from the corresponding author upon reasonable request.

Received: 17 July 2023; Accepted: 31 August 2023

Published online: 02 September 2023

## References

- Zyoud, S. E. H. *et al.* Global trends in research related to the links between microbiota and antibiotics: A visualization study. *Sci. Rep.* **13**(1), 6890 (2023).
- Hashemi, S. Y. *et al.* Degradation of ceftriaxone from aquatic solution using a heterogeneous and reusable O<sub>3</sub>/UV/Fe<sub>3</sub>O<sub>4</sub>@TiO<sub>2</sub> systems: Operational factors, kinetics and mineralisation. *Int. J. Environ. Anal. Chem.* **102**(18), 6904–6920 (2022).
- Liu, L., Xiong, X. Y., Zhang, Q., Fan, X. T. & Yang, Q. W. The efficacy of prophylactic antibiotics on post-stroke infections: An updated systematic review and meta-analysis. *Sci. Rep.* **6**(1), 36656 (2016).
- Wang, X., Jing, J., Zhou, M. & Dewil, R. Recent advances in H<sub>2</sub>O<sub>2</sub>-based advanced oxidation processes for removal of antibiotics from wastewater. *Chin. Chem. Lett.* **34**(3), 107621 (2023).
- Omufere, L. O., Maseko, B. & Olowoyo, J. O. Occurrence of antibiotics in wastewater from hospital and convectional wastewater treatment plants and their impact on the effluent receiving rivers: Current knowledge between 2010 and 2019. *Environ. Monit. Assess.* **194**(4), 306 (2022).

6. Kiani, A. *et al.* Monitoring of polycyclic aromatic hydrocarbons and probabilistic health risk assessment in yogurt and butter in Iran. *Food Sci. Nutr.* **9**(4), 2114–2128 (2021).
7. Azari, A. *et al.* Polycyclic aromatic hydrocarbons in high-consumption soft drinks and non-alcoholic beers in Iran: Monitoring, Monte Carlo simulations and human health risk assessment. *Microchem. J.* **191**, 108791 (2023).
8. Badawy, M. I., El-Gohary, F. A., Abdel-Wahed, M. S., Gad-Allah, T. A. & Ali, M. E. Mass flow and consumption calculations of pharmaceuticals in sewage treatment plant with emphasis on the fate and risk quotient assessment. *Sci. Rep.* **13**(1), 3500 (2023).
9. Peng, B. *et al.* Adsorption of antibiotics on graphene and biochar in aqueous solutions induced by  $\pi$ - $\pi$  interactions. *Sci. Rep.* **6**(1), 31920 (2016).
10. Iliopoulou, A. *et al.* Combined use of strictly anaerobic MBBR and aerobic MBR for municipal wastewater treatment and removal of pharmaceuticals. *J. Environ. Manag.* **343**, 118211 (2023).
11. Huo, J. *et al.* Iron ore or manganese ore filled constructed wetlands enhanced removal performance and changed removal process of nitrogen under sulfamethoxazole and trimethoprim stress. *Environ. Sci. Pollut. Res.* **29**(47), 71766–71773 (2022).
12. Barros, A. R. M. *et al.* Effects of the antibiotics trimethoprim (TMP) and sulfamethoxazole (SMX) on granulation, microbiology, and performance of aerobic granular sludge systems. *Chemosphere* **262**, 127840 (2021).
13. Väitalo, P., Kruglova, A., Mikola, A. & Vähälä, R. Toxicological impacts of antibiotics on aquatic micro-organisms: A mini-review. *Int. J. Hyg. Environ. Health.* **220**(3), 558–569 (2017).
14. Cui, S., Qi, Y., Zhu, Q., Wang, C. & Sun, H. A review of the influence of soil minerals and organic matter on the migration and transformation of sulfonamides. *Sci. Total Environ.* **861**, 160584 (2023).
15. Rana, S. *et al.* Recent advances in photocatalytic removal of sulfonamide pollutants from waste water by semiconductor hetero-junctions: A review. *Mater. Today Chem.* **30**, 101603 (2023).
16. Li, N. *et al.* A critical review on correlating active sites, oxidative species and degradation routes with persulfate-based antibiotics oxidation. *Water Res.* **235**, 119926 (2023).
17. Liu, M. K. *et al.* Effective removal of tetracycline antibiotics from water using hybrid carbon membranes. *Sci. Rep.* **7**(1), 43717 (2017).
18. Morrison, K. D., Misra, R. & Williams, L. B. Unearthing the antibacterial mechanism of medicinal clay: A geochemical approach to combating antibiotic resistance. *Sci. Rep.* **6**(1), 19043 (2016).
19. Ahmed, M. B., Zhou, J. L., Ngo, H. H. & Guo, W. Adsorptive removal of antibiotics from water and wastewater: Progress and challenges. *Sci. Total Environ.* **532**, 112–126 (2015).
20. Behera, M., Nayak, J., Banerjee, S., Chakraborty, S. & Tripathy, S. K. A review on the treatment of textile industry waste effluents towards the development of efficient mitigation strategy: An integrated system design approach. *J. Environ. Chem. Eng.* **9**(4), 105277 (2021).
21. Ewuzie, U. *et al.* A review on treatment technologies for printing and dyeing wastewater (PDW). *J. Water Process Eng.* **50**, 103273 (2022).
22. Bi, X. *et al.* Distribution characteristics of organic carbon (nitrogen) content, cation exchange capacity, and specific surface area in different soil particle sizes. *Sci. Rep.* **13**(1), 12242 (2023).
23. Pourabadeh, A. *et al.* Experimental design and modelling of removal of dyes using nano-zero-valent iron: a simultaneous model. *Int. J. Environ. Anal. Chem.* **100**(15), 1707–1719 (2020).
24. Shojaei, S., Nouri, A., Baharinikoo, L., Farahani, M. D. & Shojaei, S. Removal of the hazardous dyes through adsorption over nanozeolite-X: Simultaneous model, design and analysis of experiments. *Polyhedron* **196**, 114995 (2021).
25. Chan, S. S. *et al.* Prospects and environmental sustainability of phyconanotechnology: A review on algae-mediated metal nanoparticles synthesis and mechanism. *Environ. Res.* **212**, 113140 (2022).
26. Wuithschick, M., Witte, S., Kettemann, F., Rademann, K. & Polte, J. Illustrating the formation of metal nanoparticles with a growth concept based on colloidal stability. *Phys. Chem. Chem. Phys.* **17**(30), 19895–19900 (2015).
27. Ji, Q. & Li, H. High surface area activated carbon derived from chitin for efficient adsorption of crystal violet. *Diamond Relat. Mater.* **118**, 108516 (2021).
28. Abdelaziz, M. A., Owda, M. E., Abouzeid, R. E., Alaysuy, O. & Mohamed, E. I. Kinetics, isotherms, and mechanism of removing cationic and anionic dyes from aqueous solutions using chitosan/magnetite/silver nanoparticles. *Int. J. Biol. Macromol.* **225**, 1462–1475 (2023).
29. Hamza, M. F., Wei, Y., Althumayri, K., Fouda, A. & Hamad, N. A. Synthesis and characterization of functionalized chitosan nanoparticles with pyrimidine derivative for enhancing ion sorption and application for removal of contaminants. *Materials.* **15**(13), 4676 (2022).
30. Zhang, Y. *et al.* Research progress of adsorption and removal of heavy metals by chitosan and its derivatives: A review. *Chemosphere* **279**, 130927 (2021).
31. Karimi, F. *et al.* Removal of metal ions using a new magnetic chitosan nano-bio-adsorbent; A powerful approach in water treatment. *Environ. Res.* **203**, 111753 (2022).
32. Thinh, N. N. *et al.* Magnetic chitosan nanoparticles for removal of Cr (VI) from aqueous solution. *Mater. Sci. Eng.* **33**(3), 1214–1218 (2013).
33. Shen, C., Shen, Y., Wen, Y., Wang, H. & Liu, W. Fast and highly efficient removal of dyes under alkaline conditions using magnetic chitosan-Fe (III) hydrogel. *Water Res.* **45**(16), 5200–5210 (2011).
34. Shojaei, S. *et al.* Application of Taguchi method and response surface methodology into the removal of malachite green and auramine-O by NaX nanozeolites. *Sci. Rep.* **11**(1), 16054 (2021).
35. Azari, A., Nabizadeh, R., Mahvi, A. H. & Nasser, S. Magnetic multi-walled carbon nanotubes-loaded alginate for treatment of industrial dye manufacturing effluent: Adsorption modelling and process optimisation by central composite face-central design. *Int. J. Environ. Anal. Chem.* **103**(7), 1509–1529 (2023).
36. Azari, A., Nabizadeh, R., Mahvi, A. H. & Nasser, S. Integrated Fuzzy AHP-TOPSIS for selecting the best color removal process using carbon-based adsorbent materials: Multi-criteria decision making vs. systematic review approaches and modeling of textile wastewater treatment in real conditions. *Int. J. Environ. Anal. Chem.* **102**(18), 7329–7344 (2022).
37. Jradi, R., Marvillet, C. & Jeday, M. R. Analysis and estimation of cross-flow heat exchanger fouling in phosphoric acid concentration plant using response surface methodology (RSM) and artificial neural network (ANN). *Sci. Rep.* **12**(1), 20437 (2022).
38. Souadia, A., Gourine, N. & Yousfi, M. Optimization total phenolic content and antioxidant activity of *Saccocalyx satureioides* extracts obtained by ultrasonic-assisted extraction. *J. Chemom.* **36**(7), e3428 (2022).
39. Tee, W. T. *et al.* Effective remediation of lead (II) wastewater by *Parkia speciosa* pod biosorption: Box-Behnken design optimisation and adsorption performance evaluation. *Biochem. Eng. J.* **187**, 108629 (2022).
40. Zhao, J. *et al.* New use for biochar derived from bovine manure for tetracycline removal. *J. Environ. Chem. Eng.* **9**(4), 105585 (2021).
41. Wu, Y. *et al.* Enhanced sodium-ion storage with Fe<sub>3</sub>O<sub>4</sub>@Na<sub>2</sub>Ti<sub>2</sub>O<sub>7</sub> nanoleaves. *J. Solid State Chem.* **300**, 122247 (2021).
42. Norzaee, S., Bazrafshan, E., Djahed, B., Kord Mostafapour, F. & Khaksefidi, R. UV activation of persulfate for removal of penicillin G antibiotics in aqueous solution. *Sci. World J.* **2017**, 3519487 (2017).
43. Gao, Y. *et al.* Adsorption and removal of tetracycline antibiotics from aqueous solution by graphene oxide. *J. Colloid Interface Sci.* **368**(1), 540–546 (2012).
44. Wang, M. & You, X. Y. Efficient adsorption of antibiotics and heavy metals from aqueous solution by structural designed PSSMA-functionalized-chitosan magnetic composite. *Chem. Eng. J.* **454**, 140417 (2023).

45. Yang, J., Shojaei, S. & Shojaei, S. Removal of drug and dye from aqueous solutions by graphene oxide: Adsorption studies and chemometrics methods. *NPJ Clean Water*. **5**(1), 5 (2022).
46. Askari, R. *et al.* Synthesis of activated carbon from walnut wood and magnetized with cobalt ferrite (CoFe<sub>2</sub>O<sub>4</sub>) and its application in removal of cephalexin from aqueous solutions. *J. Dispersion Sci. Technol.* **44**(7), 1183–1194 (2023).
47. Lanjwani, M. F., Altunay, N. & Tuzen, M. Preparation of fatty acid-based ternary deep eutectic solvents: Application for determination of tetracycline residue in water, honey and milk samples by using vortex-assisted microextraction. *Food Chem.* **400**, 134085 (2023).
48. Vu, T. N. *et al.* Highly adsorptive removal of antibiotic and bacteria using lysozyme protein modified nanomaterials. *J. Mol. Liq.* **382**, 121903 (2023).
49. Mohammed, A. A., Kareem, S. L., Peters, R. J. & Mahdi, K. Removal of amoxicillin from aqueous solution in batch and circulated fluidized bed system using zinc oxide nanoparticles: hydrodynamic and mass transfer studies. *Environ. Nanotechnol. Monit. Manag.* **17**, 100648 (2022).
50. Chianese, S., Fenti, A., Blotvogel, J., Musmarra, D. & Iovino, P. Trimethoprim removal from wastewater: Adsorption and electro-oxidation comparative case study. *Case Stud. Chem. Environ. Eng.* **8**, 100433 (2023).
51. Li, R. *et al.* Adsorption of toxic tetracycline, thiamphenicol and sulfamethoxazole by a granular activated carbon (GAC) under different conditions. *Molecules* **27**(22), 7980 (2022).
52. Domínguez-Vargas, J. R., Gonzalez, T., Palo, P. & Cuerda-Correa, E. M. Removal of carbamazepine, naproxen, and trimethoprim from water by amberlite XAD-7: A kinetic study. *Clean: Soil, Air, Water* **41**(11), 1052–1061 (2013).
53. Mirzaei, A., Yerushalmi, L., Chen, Z. & Haghghat, F. Photocatalytic degradation of sulfamethoxazole by hierarchical magnetic ZnO@g-C<sub>3</sub>N<sub>4</sub>: RSM optimization, kinetic study, reaction pathway and toxicity evaluation. *J. Hazard. Mater.* **359**, 516–526 (2018).
54. Berges, J., Moles, S., Ormad, M. P., Mosteo, R. & Gómez, J. Antibiotics removal from aquatic environments: Adsorption of enrofloxacin, trimethoprim, sulfadiazine, and amoxicillin on vegetal powdered activated carbon. *Environ. Sci. Pollut. Res.* **28**, 8442–8452 (2021).
55. Ou, Y. *et al.* Magnetically separable Fe-MIL-88B\_NH<sub>2</sub> carbonaceous nanocomposites for efficient removal of sulfamethoxazole from aqueous solutions. *J. Colloid Interface Sci.* **570**, 163–172 (2020).

## Acknowledgements

The authors are grateful to Shiraz University for their kind support.

## Author contributions

M.A.: conceptualization, investigation, supervision, visualization, writing—review and editing. S.A.: formal analysis, investigation, visualization, writing—original draft. M.G.: formal analysis, conceptualization, validation. N.S.: methodology design, validation. M.N.: formal analysis, validation.

## Competing interests

The authors declare no competing interests.

## Additional information

**Correspondence** and requests for materials should be addressed to S.A.A.

**Reprints and permissions information** is available at [www.nature.com/reprints](http://www.nature.com/reprints).

**Publisher's note** Springer Nature remains neutral with regard to jurisdictional claims in published maps and institutional affiliations.



**Open Access** This article is licensed under a Creative Commons Attribution 4.0 International License, which permits use, sharing, adaptation, distribution and reproduction in any medium or format, as long as you give appropriate credit to the original author(s) and the source, provide a link to the Creative Commons licence, and indicate if changes were made. The images or other third party material in this article are included in the article's Creative Commons licence, unless indicated otherwise in a credit line to the material. If material is not included in the article's Creative Commons licence and your intended use is not permitted by statutory regulation or exceeds the permitted use, you will need to obtain permission directly from the copyright holder. To view a copy of this licence, visit <http://creativecommons.org/licenses/by/4.0/>.

© The Author(s) 2023